REPORT

ULTRACOLD MOLECULES

Observation of microwave shielding of ultracold molecules

Loïc Anderegg[1,2]*, Sean Burchesky[1,2], Yicheng Bao[1,2], Scarlett S. Yu[1,2], Tijs Karman[3,4], Eunmi Chae[5], Kang-Kuen Ni[1,2,6], Wolfgang Ketterle[2,7], John M. Doyle[1,2]

Harnessing the potential wide-ranging quantum science applications of molecules will require control of their interactions. Here, we used microwave radiation to directly engineer and tune the interaction potentials between ultracold calcium monofluoride (CaF) molecules. By merging two optical tweezers, each containing a single molecule, we probed collisions in three dimensions. The correct combination of microwave frequency and power created an effective repulsive shield, which suppressed the inelastic loss rate by a factor of six, in agreement with theoretical calculations. The demonstrated microwave shielding shows a general route to the creation of long-lived, dense samples of ultracold polar molecules and evaporative cooling.

Applications of ultracold molecules in quantum simulation, precision measurement, ultracold chemistry, and quantum computation (*1*, *2*) have led to rapid progress in direct cooling (*3*–*7*), assembly (*8*–*16*), trapping (*17*–*19*), and control of molecules (*20*–*23*). Engineering and control of molecular interactions will enable or enhance many of these applications. In particular, collisional interactions play a critical role in the ability to cool and, therefore, control molecules. Although there has been some success with sympathetic and evaporative cooling (*24*, *25*), these efforts have been hindered by large inelastic loss rates for both reactive and nonreactive molecular species in optical traps (*26*–*29*). Suppressing these inelastic losses, and, more generally, tuning interactions, is key to effective evaporative cooling of ultracold molecules and quantum applications.

A path to achieving this suppression is shielding, whereby molecules can be repelled from short-range distances where inelastic processes occur. Various shielding schemes for atoms (*30*–*33*) and molecules have been proposed (*34*–*39*). Recently, a scheme using dc electric fields to generate repulsive interactions was demonstrated in a two-dimensional geometry for KRb molecules (*40*). Here, we report microwave shielding of $^{40}Ca^{19}F$ molecules in three dimensions using optical tweezer traps. By tuning the microwave frequency from blue to red detuned, the system switches from shielded to "antishielded," changing the inelastic collision rate by a factor of 24, in agreement with theoretical calculations.

The microwave shielding mechanism studied here works as follows: Continuous, near-resonant microwave fields dress the molecular states, generating an oscillating dipole moment in the CaF molecule that gives rise to strong, long-range dipolar interactions (*41*). With the correct microwave dressing, this interaction is repulsive. Additionally, the dipolar interaction substantially enhances the elastic collision rate, resulting in a high elastic-to-inelastic collisional ratio, which is a key feature for evaporative cooling. In the microwave shielding scheme we used, the uppermost dressed state adiabatically converts to the repulsive branch of the dipole-dipole interaction. This repulsion leads to a classical turning point at long range (*37*, *38*) (Fig. 1A), preventing molecules from reaching short range where they would be lost with high probability (*29*). There will be residual inelastic loss at long range, predicted to be a result of nonadiabatic transitions (so-called "microwave-induced loss") (*37*, *38*). Coupled-channel calculations have shown that effective shielding requires circular polarization and high Rabi frequencies of the microwave field (*37*, *38*). Circular polarization provides coupling to the repulsive branch of the resonant dipole-dipole interaction regardless of the orientation of the collision axis relative to the molecule orientation, resulting in shielding in the bulk, that is, three dimensions. Rabi frequencies could be made high enough to create a large gap between field-dressed levels, ensuring adiabaticity during the collision.

Our experiment started from a magneto-optical trap of $^{40}Ca^{19}F$ molecules (*6*). CaF may be laser cooled, optically manipulated, and imaged owing to its closed optical cycling transitions. We used Λ-enhanced gray molasses cooling to load molecules into a conservative 1064-nm optical dipole trap (*17*, *42*).

[1]Department of Physics, Harvard University, Cambridge, MA, USA. [2]Harvard-MIT Center for Ultracold Atoms, Cambridge, MA, USA. [3]ITAMP, Harvard-Smithsonian Center for Astrophysics, Cambridge, MA, USA. [4]Radboud University, Institute for Molecules and Materials, Heijendaalseweg 135, 6525 AJ Nijmegen, Netherlands. [5]Department of Physics, Korea University, Seongbuk-gu, Seoul, Republic of Korea. [6]Department of Chemistry and Chemical Biology, Harvard University, Cambridge, MA, USA. [7]Department of Physics, Massachusetts Institute of Technology, Cambridge, MA, USA.
*Corresponding author. Email: anderegg@g.harvard.edu

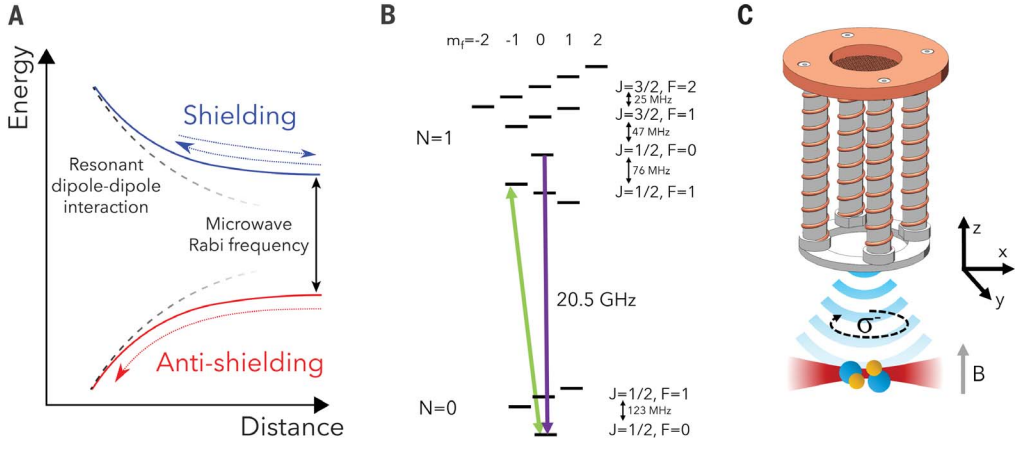

Fig. 1. Microwave shielding overview. (**A**) Diagram of the shielding process. The upper dressed state leads to a repulsive potential, preventing the molecules from reaching short range and undergoing loss. (**B**) CaF energy levels of the $X^2\Sigma^+$ electronic ground state showing the N = 1 and N = 0 rotational states separated by 20.5 GHz. The shielding transition is shown in green. The purple arrow shows the Landau-Zener sweep to the absolute ground state. (**C**) Experimental schematic showing the relative orientations of the helical antenna with respect to the tweezers. The tweezer light is linearly polarized along the *z* axis, parallel to the magnetic field *B*.

Single molecules were then transferred into two 780-nm optical tweezer traps (*43*). The tweezers had a beam waist of about 1.6 μm and a depth of 1.8 mK. Light-assisted collisions caused by the Λ-cooling light during tweezer loading ensured no more than a single molecule in each tweezer. As detailed previously (*29*), the two tweezer traps can be merged to create a colliding pair of molecules in a single trap. This merge was accomplished by using a single 780-nm laser source to create one stationary trap and by using an acousto-optical deflector to create one steerable trap. The light for these two traps was combined and then focused down, forming two tightly focused tweezer traps [radial frequency (ω_r) = $2\pi \times 91.5$ kHz] that could be merged. We measured a typical molecule temperature of 96 μK (*44*), both before and after merging. The molecules occupied many spatial modes, and therefore the collisions were three-dimensional in nature.

Once the tweezers were loaded, we applied an optical pumping pulse to populate the $|N = 1, J = 1/2, F = 0, m_f = 0\rangle$ state (Fig. 1B), where N is the rotational angular momentum, J is the total angular momentum, F is the total angular momentum including nuclear spin, and m_f is its projection onto the magnetic field. Next, we used a Landau-Zener microwave sweep to move the population to the absolute ground state $|N = 0, J = 1/2, F = 0, m_f = 0\rangle$. This transition is nominally dipole forbidden, but an applied 4-G magnetic field was mixed in the $|N = 0, F = 1, m_f = 0\rangle$ state, providing a substantial transition dipole moment. To remove any remaining population in the N = 1 rotational level, we applied a 5-ms pulse of resonant light, recoil heating the N = 1 molecules out of the tweezer trap. The two molecules, both in the ground internal state, were then merged together into a single tweezer for collisions to take place. At this point, the shielding was turned on for a variable amount of time before the tweezers were separated, and the molecules were transferred back to the N = 1 manifold for imaging. The molecules are imaged using Λ-imaging (*42*, *43*) to verify their survival.

Circularly polarized microwaves were generated by a two-by-two helical antenna array (*45*) (Fig. 1C). The helical antennas were designed for axial mode operation, creating circular polarization with a helicity set by the winding of the antenna. An array was used to increase the cleanliness of the circular polarization and the overall output power. The 20.5-GHz microwaves were generated from mixing a low–phase noise 18.5-GHz source with a 2-GHz source locked to a low-noise oscillator (*44*). The 20.5-GHz signal was then amplified and split into four paths of equal length through phase-stable cables. Each antenna had a separate 5-W microwave amplifier and a mechanical phase shifter. The microwaves propagated into a stainless-steel vacuum chamber through a glass window along the z axis, defined as the direction of the magnetic field (Fig. 1C). We determined the polarization of the microwave field by measuring the Rabi frequency of the σ^+, σ^-, and π transitions between the states $|N = 1, J = 1/2, F = 0, m_f = 0\rangle$ and $|N = 0, J = 1/2, F = 1, m_f = \pm 1, 0\rangle$. Accounting for the magnetic field–dependent matrix elements, the σ^+ and σ^- field components indicated the degree of circular polarization in the plane transverse to the axial magnetic field, and the π component of the field was related to the tilt angle of the polarization ellipse relative to the z axis. Using the measured Rabi frequencies, we then adjusted the phases of the four individual antennas to maximize the target circular field component and minimized the other two polarizations. The helical antenna array generated clean circular polarization in free space; however, the reflections from metal components in and around the vacuum chamber degraded the polarization cleanliness to a power ratio of right- to left-handed circular polarization of 100 (*44*).

To create collisional shielding, we used the $|N = 1, J = 1/2, F = 1, m_f\rangle$ hyperfine manifold, with an applied 27-G magnetic field. The magnetic field direction was such that the upper state in the manifold $|N = 1, J = 1/2, F = 1, m_f = -1\rangle$ was driven by the high-purity circular polarization. After merging the tweezers, we prepared the upper dressed state by switching on low-power microwaves with a frequency of a few megahertz blue detuned to $|N = 1, J = 1/2, F = 1, m_f = -1\rangle$. Then, adiabatically, the amplitude of the microwaves was ramped to full power in ~100 μs while the detuning remained fixed. In this way, we produced near-resonant dressing where the detuning was small with respect to the Rabi frequency. Using the highest-energy m_f level ensured that the upper dressed state did not cross any other levels as the microwave power was ramped up. The lifetime of the single-particle dressed state in the optical tweezer was limited to >500 ms by the phase noise of the microwave source.

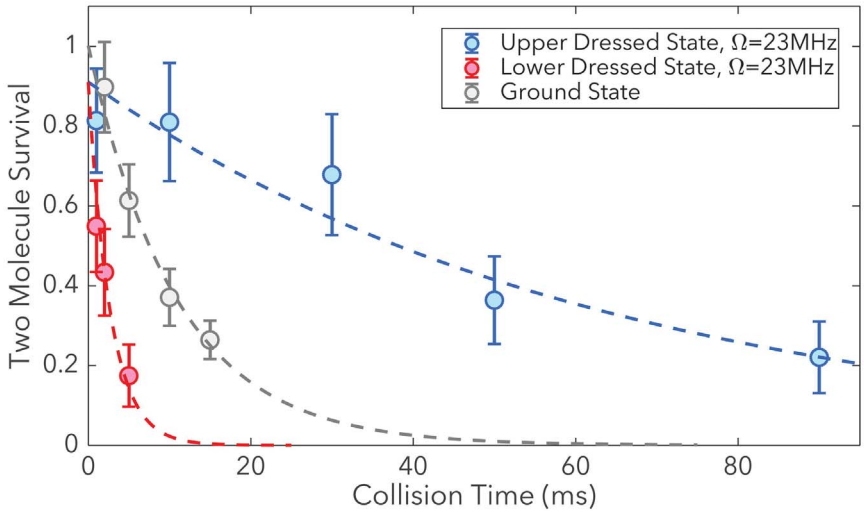

Fig. 2. Microwave shielding of CaF collisions. The gray trace (10.8 ms) shows the bare two-body loss of unshielded ground-state collisions. The blue trace (64 ms) shows the shielded loss rate at a Rabi frequency of 23 MHz and magnetic field of 27 G in the upper dressed state. The red trace (2.7 ms) shows the loss rate in the lower dressed state with a Rabi frequency of 23 MHz and magnetic field of 27 G. The error bars represent the standard error.

The collisional lifetime of the bare ground state was the reference for our shielding performance comparison. We measured the trap frequency and temperature of the bare ground state molecules to be the same as molecules prepared in the upper dressed state, thus ensuring that the densities of microwave-dressed molecules and bare ground-state molecules were comparable. The ratio of the measured lifetimes was thus the ratio of the two-body loss rates.

At a Rabi frequency of 23 MHz, and in the upper dressed state (blue detuned from the $|N = 0, F = 0, m_f = 0\rangle$ to $|N = 1, J = 1/2, F = 1, m_f = -1\rangle$ transition) in a 27-G field (Fig. 2), the shielded lifetime was 64 ms [two-body rate coefficient (β) = $7.2(2.0) \times 10^{-11}$ cm^3/s], six times longer than the bare ground-state lifetime of 10.8 ms [β = $4.2(0.8) \times 10^{-10}$ cm^3/s]. The ratio of the lifetimes was in agreement with a coupled-channel loss-rate calculation (Fig. 3). We found experimentally that the shielded lifetime was relatively independent of the polarization purity from 100:1 to 10:1 in power at a Rabi frequency of ~23 MHz (*44*).

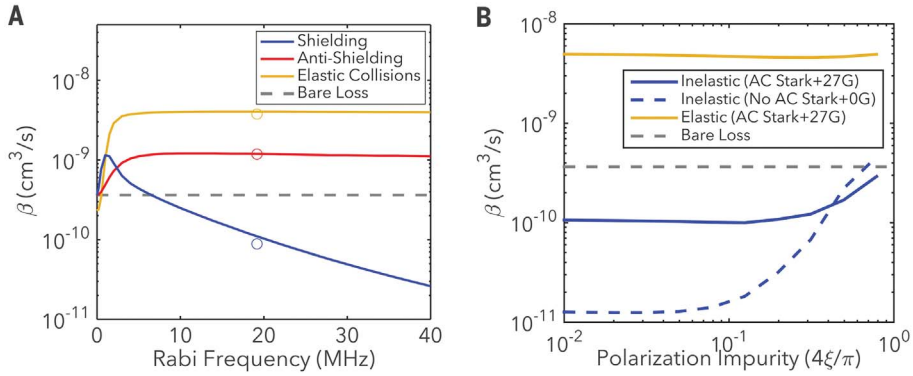

Fig. 3. Theory calculations of shielding parameters. (**A**) Rate coefficient versus Rabi frequency. Both shielding (blue) and antishielding (red) are shown. The elastic rate is shown in yellow. The solid lines are results without including spin; the circles include spin. (**B**) Plot of loss versus microwave ellipticity angle, ξ (*44*), for a Rabi frequency of 23 MHz. The tweezer trap's tensor ac Stark shift was the dominant factor reducing the effective degree of shielding. The elastic rate was nearly unaffected by the ac Stark shift and magnetic field.

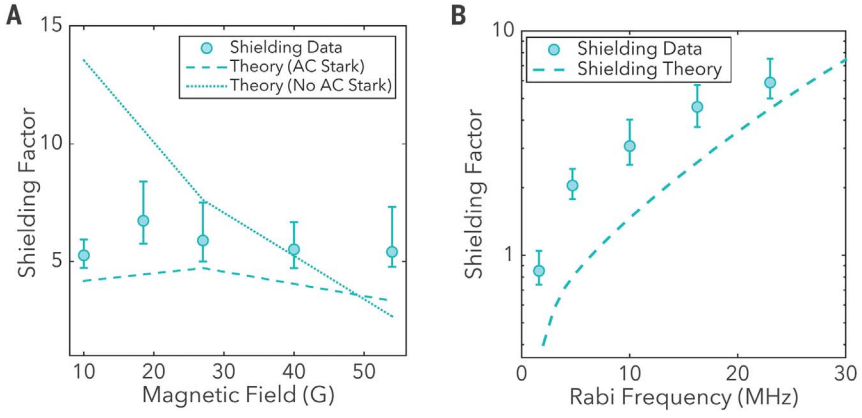

Fig. 4. Dependence of shielding on microwave power and magnetic field. The shielding factor is the ratio of the bare loss rate to the measured loss rate. (**A**) Shielding factor versus magnetic field at a Rabi frequency of 23 MHz. We found the effect of shielding to be robust over this range of magnetic fields, a result of the tensor ac Stark shift from the trap light. (**B**) Shielding factor versus Rabi frequency. We found the crossover point where shielding began to be around 3 MHz. The experimental data were taken at 27 G, and the theory curve did not include the effect of spin. The error bars represent the standard error of the fitted value.

Although the upper dressed state produced a repulsive shielding potential, the lower dressed state adiabatically connected to the attractive branch of the dipole-dipole interaction as the molecules approached during the collision, causing antishielding (*37*, *38*). Guided by this theory, we prepared the lower dressed state by flipping the direction of the magnetic field, which effectively swapped the handedness of the microwaves such that the lowest m_f level ($|N=1, J=1/2, F=1, m_f=+1\rangle$) was now the one being driven most strongly by the circularly polarized microwaves. We prepared the lower dressed state with a microwave power ramp, with the microwaves red detuned. We measured this antishielded lifetime to be 2.7 ms [$\beta = 1.7(0.5) \times 10^{-9}$ cm^3/s], faster than the bare ground state by a factor of about 4 and faster than the shielded state by a factor of 24 (see Fig. 2).

We used coupled-channel methods to calculate microwave shielding of CaF molecules. Similar to previous work (*38*), the colliding molecules were modeled as rigid rotors interacting through dipole-dipole interactions and with external magnetic and microwave fields. For details, see (*44*). In contrast to previous studies, we included the tensor ac Stark shift caused by the intense tweezer light. At short range, a fully absorbing boundary condition was imposed that yielded universal loss in the absence of microwave dressing. Nonadiabatic transitions between dressed states led to microwave-induced loss, whereby the microwave Rabi frequency was converted into kinetic energy. Short-range losses occurred to a lesser extent because the potentials involved were mainly repulsive. The results of two sets of calculations are shown in Fig. 3. First, we assumed that the microwave polarization was perfectly circular about the magnetic field and tweezer polarization directions (Fig. 3A). Cylindrical symmetry was exploited to expedite the calculations. Second, the ellipticity of the microwave polarization was added (Fig. 3B), breaking cylindrical symmetry, which made the computations more demanding such that explicitly accounting for (hyper)fine structure became intractable. Hence, we made the approximation of treating spin implicitly by an enhanced rotational *g*-factor and tested the accuracy of this approximation in Fig. 3A. As discussed in (*44*), this approximation was reasonable for low magnetic fields and in the presence of a dominant tensor ac Stark interaction.

Previous theoretical work on microwave shielding (*37*, *38*) indicated a strong dependence on the polarization. The tensor Stark shift due to the optical tweezer light aligned the molecules, which competed with the resonant dipolar interactions that lead to shielding. The coupled-channel calculations performed here indicated that this fact limited shielding for perfectly circular polarization but reduced the sensitivity to polarization imperfections (see Fig. 3B). The $|N=1, J=1/2, F=1, m_f\rangle$ hyperfine manifold, used for shielding, had a substantial tensor polarizability (*44*). The tweezer in which the collisions took place was linearly polarized along the z axis, parallel to the magnetic field and perpendicular to the plane containing the polarization ellipse of the microwaves. At a tweezer trap depth of 1.8 mK for the ground state and no applied magnetic field, we observed a splitting of 10 MHz between the $m_f = 0$ and $m_f = \pm 1$ states. This tensor Stark shift was the dominant limiting factor of the observed shielding process.

It has been shown previously (*37*) that the CaF($^2\Sigma$) fine structure can limit the effectiveness of microwave shielding, leading to losses enhanced by orders of magnitude compared with calculations neglecting (hyper)fine structure or to $^1\Sigma$ bialkali molecules, with much weaker hyperfine interactions. Here, we used the $|N=0, J=1/2, F=0\rangle \rightarrow |N=1, J=1/2, F=1\rangle$ transition, see Fig. 1A, to achieve shielding. At low magnetic fields, the electron and nuclear spins in these states are approximately coupled to a total spin singlet, which effectively eliminates the fine-structure couplings. Our calculations (Fig. 4A) predicted an enhancement of the shielding at low magnetic field but only in the absence of tensor ac Stark shifts. Including tensor ac Stark shifts, this interaction dominated the loss at low magnetic field, and the interplay between these two effects resulted in only a weak magnetic field dependence; see (*44*)

for a detailed discussion. This result was in agreement with experimentally observed shielding lifetimes that were similar for 10 to 54 G (Fig. 4A).

As predicted from theory, the shielding effect showed a clear power dependence (Fig. 4B). The loss rate increased from $\beta = 7.2(2.0) \times 10^{-11}$ cm^3/s to $\beta = 2.1(0.5) \times 10^{-10}$ cm^3/s when the microwave power was reduced from 23 to 5 MHz of Rabi frequency on the σ^- transition, keeping the polarization unchanged. Decreasing the power further to 1.5 MHz of Rabi frequency, we measured an increased loss rate of $\beta = 5.0(1.1) \times 10^{-10}$ cm^3/s, slightly higher than the bare ground state. The losses measured were almost entirely from long-range microwave-driven nonadiabatic transitions; therefore, the bare ground-state loss rate is not a lower bound (*37*, *38*). As the gap between the upper dressed state providing the repulsive potential and the lower dressed state decreased, the loss rate at low Rabi frequency was faster than the bare ground-state loss rate.

We demonstrated microwave shielding of inelastic collisions in three dimensions with ultracold CaF molecules in an optical tweezer trap. The relative ratios of experimentally measured two-body lifetimes agreed well with results of coupled-channel calculations and the qualitative features of shielding theory. By blue detuning the microwaves to prepare the shielded upper dressed state, we observed a factor of six suppression of inelastic loss relative to the bare ground state. By red detuning, we created an antishielded lower dressed state, leading to an enhanced loss rate. This shielding mechanism may be extended to a wide range of polar molecules prepared in a single quantum state (*37*, *38*), including polyatomic molecules (*46*, *47*). It is notable that the predicted elastic scattering rate with microwave dressing was greatly enhanced, leading to a ratio (γ) of elastic to inelastic rates of more than 50, which is more than enough for effective direct evaporative cooling. Theory also suggested that the shielding was limited by ac Stark shifts from the tweezer traps, indicating the possibility of improved shielding by using lower optical trap intensities.

REFERENCES AND NOTES

1. L. D. Carr, D. DeMille, R. V. Krems, J. Ye, *New J. Phys.* **11**, 055049 (2009).
2. J. L. Bohn, A. M. Rey, J. Ye, *Science* **357**, 1002–1010 (2017).
3. E. S. Shuman, J. F. Barry, D. Demille, *Nature* **467**, 820–823 (2010).
4. J. F. Barry, D. J. McCarron, E. B. Norrgard, M. H. Steinecker, D. DeMille, *Nature* **512**, 286–289 (2014).
5. S. Truppe *et al*., *Nat. Phys.* **13**, 1173–1176 (2017).
6. L. Anderegg *et al*., *Phys. Rev. Lett.* **119**, 103201 (2017).
7. A. L. Collopy *et al*., *Phys. Rev. Lett.* **121**, 213201 (2018).
8. K.-K. Ni *et al*., *Science* **322**, 231–235 (2008).
9. T. Takekoshi *et al*., *Phys. Rev. Lett.* **113**, 205301 (2014).
10. J. W. Park, S. A. Will, M. W. Zwierlein, *Phys. Rev. Lett.* **114**, 205302 (2015).
11. P. D. Gregory, J. Aldegunde, J. M. Hutson, S. L. Cornish, *Phys. Rev. A* **94**, 041403 (2016).
12. M. Guo *et al*., *Phys. Rev. A* **96**, 052505 (2017).
13. T. M. Rvachov *et al*., *Phys. Rev. Lett.* **119**, 143001 (2017).
14. L. R. Liu *et al*., *Science* **360**, 900–903 (2018).
15. W. B. Cairncross *et al*., *Phys. Rev. Lett.* **126**, 123402 (2021).
16. L. De Marco *et al*., *Science* **363**, 853–856 (2019).
17. L. Anderegg *et al*., *Nat. Phys.* **14**, 890–893 (2018).
18. H. J. Williams *et al*., *Phys. Rev. Lett.* **120**, 163201 (2018).
19. D. J. McCarron, M. H. Steinecker, Y. Zhu, D. DeMille, *Phys. Rev. Lett.* **121**, 013202 (2018).
20. S. Ospelkaus *et al*., *Phys. Rev. Lett.* **104**, 030402 (2010).
21. J. W. Park, Z. Z. Yan, H. Loh, S. A. Will, M. W. Zwierlein, *Science* **357**, 372–375 (2017).
22. F. Seeßelberg *et al*., *Phys. Rev. Lett.* **121**, 253401 (2018).
23. C. Chou *et al*., *Nature* **545**, 203–207 (2017).
24. G. Valtolina *et al*., *Nature* **588**, 239–243 (2020).
25. H. Son, J. J. Park, W. Ketterle, A. O. Jamison, *Nature* **580**, 197–200 (2020).
26. X. Ye, M. Guo, M. L. González-Martínez, G. Quéméner, D. Wang, *Sci. Adv.* **4**, eaaq0083 (2018).
27. P. D. Gregory *et al*., *Nat. Commun.* **10**, 3104 (2019).
28. M.-G. Hu *et al*., *Science* **366**, 1111–1115 (2019).
29. L. W. Cheuk *et al*., *Phys. Rev. Lett.* **125**, 043401 (2020).
30. S. Bali, D. Hoffmann, T. Walker, *Europhys. Lett.* **27**, 273–277 (1994).
31. K.-A. Suominen, M. J. Holland, K. Burnett, P. Julienne, *Phys. Rev. A* **51**, 1446–1457 (1995).
32. P. S. Julienne, *J. Res. Natl. Inst. Stand. Technol.* **101**, 487–503 (1996).
33. R. Napolitano, J. Weiner, P. S. Julienne, *Phys. Rev. A* **55**, 1191–1207 (1997).
34. A. V. Gorshkov *et al*., *Phys. Rev. Lett.* **101**, 073201 (2008).
35. G. Quéméner, J. L. Bohn, *Phys. Rev. A* **93**, 012704 (2016).
36. M. L. González-Martínez, J. L. Bohn, G. Quéméner, *Phys. Rev. A* **96**, 032718 (2017).
37. T. Karman, J. M. Hutson, *Phys. Rev. Lett.* **121**, 163401 (2018).
38. T. Karman, J. M. Hutson, *Phys. Rev. A* **100**, 052704 (2019).
39. T. Karman, *Phys. Rev. A* **101**, 042702 (2020).
40. K. Matsuda *et al*., *Science* **370**, 1324–1327 (2020).
41. Z. Z. Yan *et al*., *Phys. Rev. Lett.* **125**, 063401 (2020).
42. L. W. Cheuk *et al*., *Phys. Rev. Lett.* **121**, 083201 (2018).
43. L. Anderegg *et al*., *Science* **365**, 1156–1158 (2019).
44. See supplementary materials.
45. U. Kraft, *IEEE Trans. Antenn. Propag.* **44**, 515–522 (1996).
46. I. Kozyryev, L. Baum, K. Matsuda, J. M. Doyle, *Chem. Phys. Chem.* **17**, 3641–3648 (2016).
47. D. Mitra *et al*., *Science* **369**, 1366–1369 (2020).
48. L. Anderegg, S. Burchesky, Y. Bao, S. S. Yu, T. Karman, E. Chae, K.-K. Ni, W. Ketterle, J. M. Doyle, Data for observation of microwave shielding of ultracold molecules. Zenodo (2021); https://doi.org/10.5281/zenodo.4724359.

ACKNOWLEDGMENTS

Funding: This work was supported by the US Army Research Office, US Department of Energy, and National Science Foundation (NSF). L.A. acknowledges support from the Harvard Quantum Initiative. S.B. and S.S.Y. acknowledge support from the NSF Graduate Research Fellowships Program. E.C. is supported by National Research Foundation of Korea (2021R1C1C1009450 and 2020R1A4A1018015). **Author contributions:** L.A., S.B., Y.B., S.S.Y., E.C., K.-K.N., W.K., and J.M.D. contributed to the experimental effort. T.K. performed the theoretical calculations. All authors discussed the results and contributed to the manuscript. **Competing interests:** None declared. **Data and materials availability:** All data needed to evaluate the conclusions in this paper are present in the paper or in the supplementary materials. All data presented in this paper are deposited at Zenodo (*48*).

SUPPLEMENTARY MATERIALS

science.sciencemag.org/content/373/6556/779/suppl/DC1
Supplementary Text
Figs. S1 to S7
References (*49*–*52*)

9 February 2021; accepted 7 July 2021
10.1126/science.abg9502

Observation of microwave shielding of ultracold molecules

Loïc Anderegg, Sean Burchesky, Yicheng Bao, Scarlett S. Yu, Tijs Karman, Eunmi Chae, Kang-Kuen Ni, Wolfgang Ketterle and John M. Doyle

Science **373** (6556), 779-782.
DOI: 10.1126/science.abg9502

Shielding ultracold molecules

Ultracold molecules hold promise for a wide range of exciting applications. However, such applications are currently hampered by the limited number of ultracold molecular ensembles that can be created and by their short lifetimes. Anderegg *et al.* used a microwave dressing field to tune the collisional properties of calcium monofluoride molecules trapped in optical tweezers. This approach allowed a sixfold suppression of inelastic trap-loss collisions. This scheme paves the way for the creation of a variety of long-lived ultracold molecular ensembles.

Science, abg9502, this issue p. 779